Available online at www.sciencedirect.com
ScienceDirect
Journal of Photochemistry and Photobiology A: Chemistry 188 (2007) 287–292
Journal of Photochemistry and Photobiology A:Chemistry
www.elsevier.com/locate/jphotochem

Theoretical studies on spectroscopic properties of binuclear palladium(II) halide with phosphine ligands

Qing-Jiang Pan [a], Xin Zhou [b], Hong-Xing Zhang [b,*], Hong-Gang Fu [a,*]

[a] *Laboratory of Physical Chemistry, School of Chemistry and Materials Science, Heilongjiang University, Harbin 150080, China*
[b] *State Key Laboratory of Theoretical and Computational Chemistry, Institute of Theoretical Chemistry, Jilin University, Changchun 130023, China*

Received 31 July 2006; received in revised form 27 October 2006; accepted 13 December 2006
Available online 20 December 2006

Abstract

The structures of *trans*-$[Pd_2X_4(PH_2CH_2PH_2)_2]$ (X = Cl (**1**), Br (**2**) and I (**4**)) and $[Pd_2(\mu\text{-}I)_2I_2(PH_2CH_2PH_2)_2]$ (**3**) in the ground and excited states were optimized by the MP2 and unrestricted MP2 methods. It is shown that upon excitation the Pd–Pd distances shorten ca. 0.40 Å for **1**, **2** and **4** but lengthen ca. 0.10 Å for **3**. This is rationalized by their electronic structures in the excited states and spectroscopic calculations. On the basis of such structures, we predict the absorption and emission spectra of **1–3** in the $CHCl_3$ solution at the time-dependent density functional theory (TD-DFT) level. Experimental absorption spectra are well reproduced by theoretically simulated spectra.

Keywords: Palladium(II) complexes; Spectroscopic properties; Excited state

1. Introduction

Binuclear d^8 complexes have attracted considerable attention from synthetic and material chemists because of their novel structural characteristics and also because of the possibility of their distinct solid state properties [1]. The d^8 metal such as Pt(II), Pd(II) usually forms the square-planar tetracoordinate structures with a wide range of ligands, resulting in an abundance of complexes [1–10]. The discovery of the famous complex, $[Pt_2(pop)_4]^{4-}$ ($pop = P_2O_5H_2^{2-}$) [9,10], greatly motivates researchers to seek the promising optical materials. Extensive spectroscopic investigations have indicated that the triplet excited state, $[Pt_2(pop)_4]^{4-*}$, can abstract hydrogen atoms from a wide range of substrates, including alcohols, hydrocarbons, silanes and stannanes, as well as halogen atoms from alkyl and aryl halides [9–11].

Special attention has been focused on the spectroscopic and structural properties of binuclear palladium(II) complexes [12–18]. For example, *trans*-$[Pd_2X_4(PR_2CH_2PR_2)_2]$ (X = Cl and Br, R = Me and Et; X = CN, R = Me, Cy and Ph) has been structurally characterized with a well-known Pd–Pd distance in the range of 3.0–3.3 Å [16–18]. Their featured absorption and emission spectra are closely related to the halogen atoms and/or the palladium atoms. Despite their interesting photoluminescent and excited state properties, few theoretical attempts were made on the binuclear palladium(II) complexes [17,19].

So far, computational methods are sufficiently advanced to allow calculation of excited states of large molecules [11,20–22]. Associated with the accurate experimental results, it is possible to investigate systematically spectroscopic properties of transition metal complexes in theory. In the paper, the second-order Møller-Plesset perturbation (MP2) [23] and unrestricted MP2 (UMP2) optimizations were performed for *trans*-$[Pd_2X_4(PH_2CH_2PH_2)_2]$ (X = Cl (**1**), Br (**2**) and I (**4**)) and $[Pd_2(\mu\text{-}I)_2I_2(PH_2CH_2PH_2)_2]$ (**3**) in the ground and triplet excited states, respectively. Their absorption and emission spectra estimated by the time-dependent density functional theory (TD-DFT) [24–26] were discussed in detail.

1.1. Computational details

In the calculations, we used **1–3** to replace the real complexes *trans*-$[Pd_2X_4(PR_2CH_2PR_2)_2]$ and $[Pd_2(\mu\text{-}I)_2I_2(PR_2CH_2PR_2)_2]$ (X = Cl and Br; R = Me and Et) [18].

* Correspondence to: Professor Hong-Gang Fu, School of Chemistry and Materials Science, Heilongjiang University, China. Tel.: 86 451 86608545; Professor Hong-Xing Zhang, Institute of Theoretical Chemistry, Jilin University, China. Tel.: 86 431 8498966.
E-mail addresses: panqjitc@163.com (Q.-J. Pan), zhanghx@mail.jlu.edu.cn (H.-X. Zhang), fuhg@vip.sina.com (H.-G. Fu).

1010-6030/$ – see front matter © 2006 Elsevier B.V. All rights reserved.
doi:10.1016/j.jphotochem.2006.12.024

The similar model was applied in many works to save the computational resources [20,21,27,28]. Although a face-to-face complex, *trans*-$[Pd_2I_4(PR_2CH_2PR_2)_2$, are not found in experiment, we theoretically optimize its structure. Furthermore, we explored the relative stabilities of **3** and **4** as well as $[Pd_2(\mu\text{-}I)_2I_2(PMe_2CH_2PMe_2)_2]$ (**5**) and *trans*-$[Pd_2I_4(PMe_2CH_2PMe_2)_2]$ (**6**). The C_{2h} symmetry was adopted for **1**–**6** in the calculations, consistent with the X-ray diffraction crystal structures available [18].

All the calculations were carried out using the GAUSSIAN03 program package [29]. We used the effective core potentials (ECPs) of Hay and Wadt [30,31] for Pd, Cl, Br, I and P atoms. The LanL2DZ basis sets associated with the ECPs were employed. In order to describe the molecular properties precisely, one additional function was implemented for Cl ($\alpha_d = 0.514$), Br ($\alpha_d = 0.389$), I ($\alpha_d = 0.266$) and P ($\alpha_d = 0.34$) [32]. The ground- and triplet excited-state structures of **1**–**4** were optimized by the MP2 and UMP2 methods, respectively. Based on the optimized structures of **1**–**3**, we performed the Polarized Continuum Model (PCM) [33] calculations at the TD-DFT level to predict absorption and emission spectra in the $CHCl_3$ solution. According to these results, we simulated their absorption spectra using the Gaussian curve to compare with the reported spectra [18].

2. Results and discussion

2.1. Geometry optimizations on *1*–*4*

Selected results from the geometry optimizations on **1**–**4** are listed in Table 1, compared with values of the X-ray crystal diffraction of *trans*-$[Pd_2X_4(PMe_2CH_2PMe_2)_2]$ (X = Cl and Br) and $[Pd_2(\mu\text{-}I)_2I_2(PMe_2CH_2PMe_2)_2]$ [18]. Their structures are displayed in Fig. 1 with the depicted coordinate orientation.

In the ground state, the MP2 optimized and experimental geometry parameters for **1**–**3** are very close, although deviations between theory and experiment are found for Pd–Pd distances. For example, the calculated Pd–P and Pd–X bond lengths are well comparable to experimental values with the largest difference of 0.045 Å. In the calculations, the P–Pd–P angle of 176°–177° and X–Pd–X angle of 160°–171° for **1**,**2** and **4** indicate that the Pd(II) atom takes the square-planar geometry, close to experimental 175° and 170° (mean value), respectively. We predict the X–Pd–Pd angles of the three complexes at 94.7°, 96.9° and 100.1°. This is consistent with the increasing repulsion along Cl < Br < I in the face-to-face conformations. In contrast, the Pd(II) atom of **3** forms five-coordination geometry.

An interesting structural feature for the binuclear metal complexes is the shorter metal–metal separation. The calculated Pd(II)–Pd(II) distances of **1**–**4** are 3.240, 3.234, 2.759 and 3.192 Å. The first three are comparable to experimental distances of 3.352, 3.350 and 2.908 Å [18], respectively. Despite such a large difference, all the Pd–Pd distances are shorter than the sum of the van der Waals radii (3.50 Å) [34], an important indicator whether the metal–metal interaction occurs or not. So our calculations can present a reasonable description for **1**–**4**. For a ring-skeleton structure complex, the bridging ligands pull the two metal atoms in a closer distance, which results in the compulsive metal–metal interaction. So the metal–metal interaction should be explicitly divided into compulsive and attractive (bonding) interactions. To explore whether the Pd–Pd interaction in **1**–**4** is bonding or not, the frequency calculations were carried out at the MP2 level. Through carefully examining the vibrational modes, no Pd–Pd stretching vibration is found. Therefore, we conclude that no metal–metal bonding interaction is present, consistent with experimental reports [18].

In experiment, the face-to-face conformation complexes, *trans*-$[Pd_2X_4(PMe_2CH_2PMe_2)_2]$, were synthesized for the chloride and bromide but the bridging conformation, $[Pd_2(\mu\text{-}I)_2I_2(PMe_2CH_2PMe_2)_2]$, for the iodide. The optimizations on isomers, **3** and **4** as well as **5** and **6** (Table 1 and S-Table 1 of

Table 1
Optimized geometry parameters of *trans*-$[Pd_2X_4(PH_2CH_2PH_2)_2]$ (X = Cl (**1**), Br (**2**) and I (**4**)) and $[Pd_2(\mu\text{-}I)_2I_2(PH_2CH_2PH_2)_2]$ (**3**) in the ground and excited states using the MP2 and UMP2 methods, respectively

Parameters[a]	**1**			**2**			**3**			**4**	
	^1A_g	Exp.[b]	^3A_u	^1A_g	Exp.[b]	^3A_u	^1A_g	Exp.[b]	^3B_g	^1A_g	^3A_u
Bond length (Å)											
Pd–Pd	3.240	3.352	2.841	3.234	3.350	2.824	2.759	2.908	2.854	3.192	2.814
Pd–P	2.316	2.313	2.348	2.314	2.317	2.331	2.303	2.304	2.322	2.316	2.312
P–C	1.874		1.871	1.876		1.871	1.879		1.891	1.877	1.873
Pd–X	2.333	2.305	2.378	2.475	2.435	2.509				2.655	2.663
Pd–X_a							2.684	2.673	2.719		
Pd–X_b							2.881	2.847	2.821		
P···P	3.089		2.912	3.090		2.902	3.106		3.186	3.083	2.898
Bond angle (°)											
P–Pd–P	176.2	174.9	178.3	176.4	174.8	178.1	171.4	174.2	171.8	177.3	177.9
P–Pd–Pd	88.1		90.9	88.2		91.0	94.3		94.1	88.6	91.0
X–Pd–X	170.6	173.9	159.3	166.2	168.3	154.5				159.7	149.9
X–Pd–Pd	94.7		100.4	96.9		102.7	61.4		59.6	100.1	105.1
X–Pd–P	86.2	87.4	85.0	87.2	88.3	86.6				87.9	87.9
X–Pd–P′	94.1	93.0	94.7	93.2	92.3	92.9				92.6	91.6

[a] X: the halogen atom in the face-to-face isomer; X_a: the iodine atom on the axis of Pd–Pd; X_b: the iodine atom bridging the two palladium(II) atoms.
[b] Experimental values from Ref. [18].

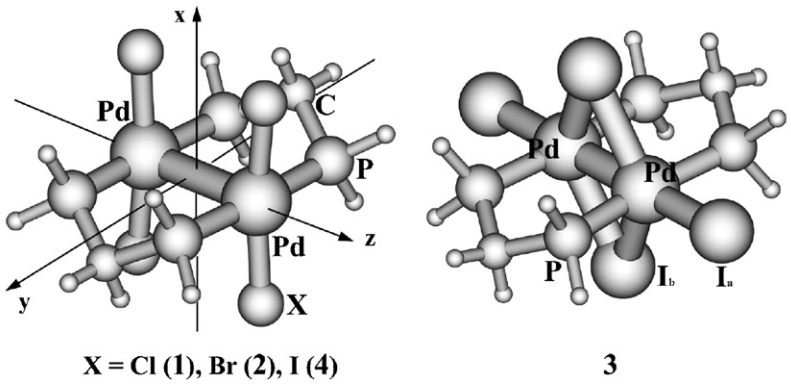

Fig. 1. Geometry structures of *trans*-$[Pd_2X_4(PH_2CH_2PH_2)_2]$ (X = Cl (**1**), Br (**2**) and I (**4**)) and $[Pd_2(\mu\text{-}I)_2I_2(PH_2CH_2PH_2)_2]$ (**3**).

Supplementary Materials) reveal the reason. The single-point energy calculations using the higher-level MP4 method demonstrate that the total energies of bridging conformation complexes (**3/5**) are lower than those of face-to-face conformation complexes (**4/6**). Therefore, the bridging isomer is relatively stable for the palladium(II) iodide complex.

Compared with those in the ground states, the geometry parameters in the triplet excited states change greatly. Upon excitation, the Pd–Pd distances shrink by ca. 0.40 Å, the Pt–P bonds lengthen ca. 0.03 Å and the Pt–X bonds lengthen ca. 0.04 Å for face-to-face conformation **1**,**2** and **4**; however, the elongation occurs in the Pd–Pd distance of **3**. This should be correlated with the promotion of electron into bonding or antibonding orbitals between the two Pd atoms.

2.2. Absorption spectra of *1–3* in the $CHCl_3$ solution

The combined calculations of TD-DFT (B3LYP) and PCM on **1**–**3** were carried out to explore the transition properties of absorption spectra in the $CHCl_3$ solution. The calculated transition energies (cm^{-1}) and oscillator strengths are listed in Table 2, S-Table 2 and S-Table 3, together with the experimental spectral data [18]. At the same time, the compositions of the frontier molecular orbitals are summarized in S-Tables 4–6.

In Fig. 2, we have simulated the absorption spectra of **1** in solution on the basis of the TD-DFT/PCM calculations. The theoretical spectra of **1** contain an intense absorption at 29,760 cm^{-1} and a weak peak at 23,150 cm^{-1}. The experimental spectra for *trans*-$[Pd_2Cl_4(PR_2CH_2PR_2)_2]$ (R = Me and Et) [18] exhibit absorption bands at 31,850 cm^{-1} (10,400 $M^{-1}\,cm^{-1}$) and 26,460 cm^{-1} (2500 $M^{-1}\,cm^{-1}$) (Fig. 2). Apparently, the general spectral pattern of experimental spectra (dashed line) is well reproduced by the calculated results (solid line). Our studies reveal the lower-energy absorptions are dominated by the $d \rightarrow d$ and $Cl \rightarrow Pd$ charge transfer (LMCT) transitions (Table 2 and S-Table 4). Most orbitals in **1** mainly arise from the Pd 4d and Cl 3p contributions. The calculated absorption at 29,760 cm^{-1} has the largest oscillator strength of 0.112 and is contributed by the $11b_g \rightarrow 13a_u$ and $14b_u \rightarrow 16a_g$ configurations. According to S-Table 4, the p_y(Cl) compositions are predominant in $11b_g$ and $14b_u$ while $13a_u$ and $16a_g$ have significant $d_{x^2-y^2}$ (Pd) characters. Thus, the absorption was attributed

Table 2
Calculated absorptions of **1** in the $CHCl_3$ solution at the TD-DFT (B3LYP) level, associated with the absorptions observed in the experiment

States	Conf.	|CI Coeff.| > 0.2	Transition energy (cm^{-1})	f^a	Exp. (R = Me)[b]	Exp. (R = Et)[b]
A^1B_u	$12b_g \rightarrow 13a_u$	0.589	21,010	0.001		
	$15b_u \rightarrow 16a_g$	0.314				
B^1A_u	$12a_u \rightarrow 16a_g$	0.646	23,150	0.009	26,460 (2500)	26,320 (2300)
C^1B_u	$11b_g \rightarrow 13a_u$	0.478	29,760	0.112	31,850 (10,400)	31,250 (12,300)
	$14b_u \rightarrow 16a_g$	0.449				
D^1B_u	$14b_u \rightarrow 16a_g$	0.513	31,650	0.001		
	$11b_g \rightarrow 13a_u$	−0.488				
E^1B_u	$9b_g \rightarrow 13a_u$	0.563	33,560	0.008		
	$12b_u \rightarrow 16a_g$	0.308				
F^1A_u	$14a_g \rightarrow 13a_u$	0.553	35,340	0.005		
	$13a_g \rightarrow 13a_u$	−0.330				
	$10a_u \rightarrow 16a_g$	−0.203				

[a] Oscillator strength.
[b] Experimental absorptions of *trans*-$[Pd_2Cl_4(PR_2CH_2PR_2)_2]$ (R = Me and Et) from Ref. [18], and molar absorption coefficient ($M^{-1}\,cm^{-1}$) listed between parentheses.

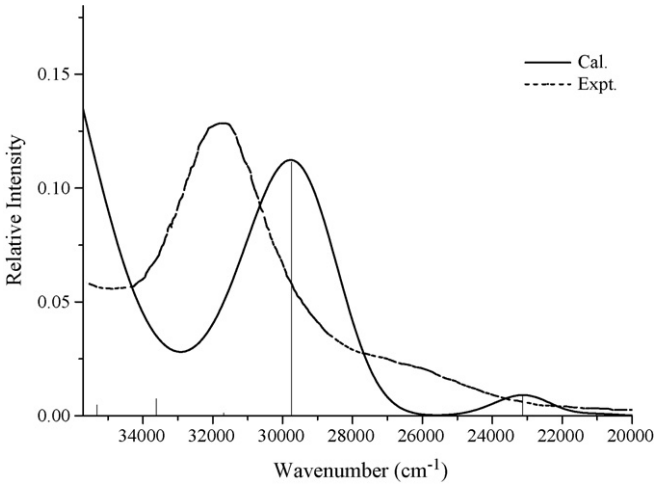

Fig. 2. Simulated absorption spectra in water for **1** from the TD-DFT/PCM calculations, together with experimental spectra from Ref. [18].

to a p_y(Cl) → $d_{x^2-y^2}$(Pd) charge transfer (LMCT) transition. This agrees with experimental assignment for the most intense absorption peak [18]. Our calculations show that the A^1B_u, B^1A_u and E^1B_u excited states give rise to the $d_{xz} \rightarrow d_{x^2-y^2}$, $d_{z^2} \rightarrow d_{x^2-y^2}$ and $d_{yz} \rightarrow d_{x^2-y^2}$ transition absorptions, respectively; however, the 35,340 cm^{-1} absorption has the admixture of the d → d and LMCT transitions.

Similar simulation of absorption spectra for **2** was performed according to the TD-DFT/PCM results (a solid line in S-Fig. 1), together with the experimental spectra (dashed line in S-Fig. 1). Compared with our calculations on **1**, although the frontier molecular orbitals of **2** also are composed primarily of the Pd d and Br p orbitals, the contributions of Br atoms apparently increase. This is related to the donating ability of Br > Cl. Consequently, the LMCT increases while the d → d decreases in the absorptions of **2**. For the bromide complex, the theoretically simulated absorption spectra possess three peaks at 32,680 (shoulder), 25,250 and 20,700 cm^{-1}. Among these, the last two absorptions correspond to the experimental absorption bands. According to S-Tables 2 and 5, we attributed the two absorptions to p_y(Br) → $d_{x^2-y^2}$(Pd) (LMCT) and $d_{z^2} \rightarrow d_{x^2-y^2}$ transitions, respectively.

Because of its structural characteristics in having bridging iodine atoms, simulated spectra of **3** are apparently different from those of **1** and **2**. S-Fig. 2 (solid line) illustrates that the theoretical spectra of **3** contain four absorption bands at 30,960, 25,250, 18,450 and 16,370 cm^{-1}, more complex than those of **1** and **2**. Because, the donating ability increases on going from Cl, Br to I, the frontier molecular orbitals of **3** possess predominant p compositions of I atoms mixed with the Pd d orbitals. Therefore, the LMCT transitions are dominant in absorption transitions as shown in S-Tables 3 and 6. Reasonable agreement is found between the simulated and experimental spectra (S-Fig. 2). We related our calculated absorptions to experimental 31,250, 26,460, 18,730 and 16,080 cm^{-1} of *trans*-$[Pd_2(\mu\text{-}I)_2I_2(PR_2CH_2PR_2)_2]$ (R = Me and Et) [18], respectively. The three lower-energy absorptions were assigned as LMCT mixed with the $d \rightarrow d$ transitions, while the higher-energy absorption favors the d → d transition properties.

2.3. Emission spectra of *1–3*

To explore the emissive properties of **1–3**, we performed the TD-DFT calculations on the basis of the triplet excited-state structures. Emission energies (cm^{-1}) in the gas phase and $CHCl_3$ solution are listed in Table 3. The configurations contributing to the emissions and their CI coefficients in the wave functions are very similar in the two media. Compared with that in the gas phase, the solvent effect results in 200–600 cm^{-1} blue shift of emission energies.

For the face-to-face complexes **1** and **2**, they have identical ^3A_u excited-state symmetry and $12a_u \rightarrow 16a_g$ excitation configuration; however, the different case occurs in **3** with the bridging iodine ligands. We present the compositions of the molecular orbitals involved in the emissive transitions in S-Table 7. For **1**, it is shown in the gas phase that $12a_u$ (HOMO) is composed of 61.6% d_{z^2} and 28.0% p_z(Cl) and $16a_g$ (LUMO) is formed by 35.9% $d_{x^2-y^2}$, 21.4% p_x(Cl) and 13.6 s(P). For the emissive process, the electron should transfer from the triplet excited state to the ground state. So, the gas phase emission at 12,450 cm^{-1} was attributed to the $d_{x^2-y^2} \rightarrow d_{z^2}$ transition with some P → Pd charge transfer (LMCT). In the

Table 3
TD-DFT calculated emission energies (cm^{-1}) of **1–3** in the gas phase and $CHCl_3$ solution based on the UMP2 optimized structures

Complexes	State	Medium	Emission energy (cm^{-1})	Conf.	|CI Coeff.| > 0.2
1	^3A_u	Gas	12,450	$12a_u \rightarrow 16a_g$	0.724
	^3A_u	Solution	12,720	$12a_u \rightarrow 16a_g$	0.730
2	^3A_u	Gas	11,740	$12a_u \rightarrow 16a_g$	0.719
	^3A_u	Solution	11,950	$12a_u \rightarrow 16a_g$	0.720
3	^3B_g	Gas	15,650	$15b_u \rightarrow 12a_u$	0.582
				$10b_g \rightarrow 17a_g$	0.385
				$14b_u \rightarrow 12a_u$	−0.212
	^3B_g	Solution	16,260	$15b_u \rightarrow 12a_u$	0.566
				$10b_g \rightarrow 17a_g$	0.381
				$14b_u \rightarrow 12a_u$	−0.256

excited state of **1**, the Pd–Pd distance is predicted at 2.841 Å. At such a short distance, the Pd–Pd bonding interaction is present, which is reflected in the bonding $16a_g$ (LUMO) orbital. Therefore, the 12,450 cm^{-1} emission was further attributed to the $\delta(d_{x^2-y^2}) \rightarrow \sigma^*(d_{z^2})$ mixed with LMCT transitions. When the solvent effect is considered in the calculations, the emission blue-shifts to 12,720 cm^{-1}. The interaction of **1** with the solvent molecules stabilizes both $12a_u$ and $16a_g$ orbitals relative to those in the gas phase, but the stabilization energy is more for the former. The solution emission also arises from the $\delta(d_{x^2-y^2}) \rightarrow \sigma^*(d_{z^2})$ transition mixed with the P → Pd charge transfer (LMCT). Similar analyses demonstrate that emissions of **2** have similar $\delta(d_{x^2-y^2}) \rightarrow \sigma^*(d_{z^2})$ and LMCT transitions except for the increase of bromine participations in the $12a_u$ and $16a_g$ orbitals.

In contrast to those of **1** and **2**, emission of **3** has relatively complex excitation configurations. The $15b_u \rightarrow 12a_u$, $10b_g \rightarrow 17a_g$ and $14b_u \rightarrow 12a_u$ configurations contribute to the emissions at 15,650 and 16,260 cm^{-1} in the gas phase and solution, respectively. Through the S-Table 7, the occupied $15b_u$, $10b_g$ and $14b_u$ orbitals possess the predominant iodine characters (>70%) while the unoccupied $12a_u$ and $17a_g$ orbitals are composed of the Pd d orbital, phosphine ligand and iodine ligand. Among these orbitals, analyses on the wave functions of the excited state show that $12a_u$ possesses the σ antibonding characters. Therefore, we assigned the emissions of **3** as $\sigma^*(d_{x^2-y^2}, d_{z^2}) \rightarrow p_y(I)$ (MLCT) and phosphine → $p_y(I)$ (LLCT) transitions from the triplet excited state to the ground state.

3. Conclusions

To explore spectroscopic properties of binuclear palladium(II) complexes, the structures of **1–4** in the ground and triplet excited states were optimized by the MP2 and UMP2 methods. It is shown that upon excitation the Pd–Pd distances greatly shorten ca. 0.40 Å for **1**, **2** and **4** but lengthen ca. 0.10 Å for **3**. The subsequent spectroscopic studies reveal the promotion of electron into Pd–Pd bonding orbitals for the former and into Pd–Pd antibonding orbital for the latter.

On the basis of their optimized ground-state structures, we predict absorption spectra of **1–3** in the $CHCl_3$ solution at the TD-DFT level. The simulated absorption spectra are in reasonable agreement with experimental measurements. The most intense peak observed in experiment was theoretically attributed to $p_y(X) \rightarrow d_{x^2-y^2}$(Pd) (LMCT) for **1** and **2** and LMCT/d → d transitions for **3**, consistent with experimental assignments. The studies on the electronic absorptions indicate the halogen contributions apparently increase on going from **1–3** due to the increase of the donating ability from Cl–I. Under the excited-state structures, TD-DFT predicts the phosphorescent emissions of **1–3** at 12,450, 11,740 and 15,650 cm^{-1} in the gas phase, attributed to the, $\delta(d_{x^2-y^2}) \rightarrow \sigma^*(d_{z_2})$ and $\sigma^*(d_{x^2-y^2}, d_{z^2}) \rightarrow$ I transitions, respectively. The introduction of the solvent effect results in 200–600 cm^{-1} blue shift of the emissions but does not change their transition properties.

Acknowledgement

This work is supported by the National Natural Science Foundation of China (No. 20173021, 20431030, 20573042 and 20671032), the Natural Science Foundation of Heilongjiang Province of China (No. B200601), and the Science Foundation for Excellent Youth of Heilongjiang University of China (JC2006L2).

Appendix A. Supplementary data

Supplementary data associated with this article can be found, in the online version, at doi:10.1016/j.jphotochem.2006.12.024.

References

[1] V.K. Jain, L. Jain, Coord. Chem. Rev. 249 (2005) 3075–3197.
[2] J.L. Neto, G.M. de Lima, H. Beraldo, Spectrochim. Acta A 63 (2006) 669–672.
[3] L. Barloy, S. Ramdeehul, J.A. Osborn, C. Carlotti, F. Taulelle, A. de Cian, J. Fischer, Eur. J. Inorg. Chem. (2000) 2523–2532.
[4] V.W.-W. Yam, C.-H. Tao, L. Zhang, K.M.-C. Wong, K.-K. Cheung, Organometallics 20 (2001) 453–459.
[5] B.-C. Tzeng, W.-F. Fu, C.-M. Che, H.-Y. Chao, K.-K. Cheung, S.-M. Peng, J. Chem. Soc., Dalton Trans. (1999) 1017–1023.
[6] F.S.M. Hassan, D.P. Markham, P.G. Pringle, B.L. Shaw, J. Chem. Soc., Dalton Trans. (1985) 279–283.
[7] W.R. Mason III, H.B. Gray, J. Am. Chem. Soc. 90 (1968) 5721–5729.
[8] H. Kunkely, A. Vogler, J. Photochem. Photobiol. A 114 (1998) 193–195.
[9] A.P. Zipp, Coord. Chem. Rev. 84 (1988) 47–83.
[10] D.M. Roundhill, H.B. Gray, C.-M. Che, Acc. Chem. Res. 22 (1989) 55–61.
[11] I.V. Novozhilova, A.V. Volkov, P. Coppens, J. Am. Chem. Soc. 125 (2003) 1079–1087.
[12] R.A. Stockland Jr., M. Janka, G.R. Hoel, N.P. Rath, G.K. Anderson, Organometallics 20 (2001) 5212–5219.
[13] M.K. Richmond, S.L. Scott, G.P.A. Yap, H. Alper, Organometallics 21 (2002) 3395–3400.
[14] M. Cera, C. Cerrada, M. Laguna, J.A. Mata, H. Teruel, Organometallics 21 (2002) 121–126.
[15] C.-M. Che, F.H. Herbstein, W.P. Schaefer, R.E. Marsh, Inorg. Chem. 23 (1984) 2572–2575.
[16] H.-K. Yip, T.-F. Lai, C.-M. Che, J.Chem. Soc., Dalton Trans. (1991) 1639–1641.
[17] B.-H. Xia, C.-M. Che, Z.-Y. Zhou, Chem. Eur. J. 9 (2003) 3055–3064.
[18] C.B. Pamplin, S.J. Rettig, B.O. Patrick, B.R. James, Inorg. Chem. 42 (2003) 4117–4126.
[19] F.A. Cotton, M. Matusz, R. Poli, X. Feng, J. Am. Chem. Soc. 110 (1988) 1144–1154.
[20] Q.-J. Pan, H.-X. Zhang, Chem. Phys. Lett. 294 (2004) 155–160.
[21] Q.-J. Pan, H.-X. Zhang, Inorg. Chem. 43 (2004) 593–601.
[22] X. Wang, W. Wang, M. Koyama, M. Kubo, A. Miyamoto, J. Photochem. Photobiol. A 179 (2006) 149–155.
[23] C. Møller, M.S. Plesset, Phys. Rev. 46 (1934) 618–622.
[24] M.E. Casida, C. Jamorski, K.C. Casida, D.R. Salahub, J. Chem. Phys. 108 (1998) 4439–4449.
[25] R.E. Statmann, G.E. Scuseria, J. Chem. Phys. 109 (1998) 8218–8224.
[26] R. Bauernschmitt, R. Ahlrichs, Chem. Phys. Lett. 256 (1996) 454–464.
[27] E.J. Fernández, M.C. Gimeno, P.G. Jones, A. Laguna, M. Laguna, J.M. López-de-Luzuriaga, M.A. Rodriguez, Chem. Ber. 128 (1995) 121–124.
[28] O.D. Häberlen, N. Rösch, J. Phys. Chem. 97 (1993) 4970–4973.
[29] M.J. Frisch, G.W. Trucks, H.B. Schlegel, G.E. Scuseria, M.A. Robb, J.R. Cheeseman, J.A. Montgomery Jr., T. Vreven, K.N. Kudin, J.C. Burant, J.M. Millam, S.S. Iyengar, J. Tomasi, V. Barone, B. Mennucci, M. Cossi, G. Scalmani, N. Rega, G.A. Petersson, H. Nakatsuji, M. Hada, M. Ehara, K. Toyota, R. Fukuda, J. Hasegawa, M. Ishida, T. Nakajima, Y. Honda, O. Kitao, H.

Nakai, M. Klene, X. Li, J.E. Knox, H.P. Hratchian, J.B. Cross, C. Adamo, J. Jaramillo, R. Gomperts, R.E. Stratmann, O. Yazyev, A.J. Austin, R. Cammi, C. Pomelli, J.W. Ochterski, P.Y. Ayala, K. Morokuma, G.A. Voth, P. Salvador, J.J. Dannenberg, V.G. Zakrzewski, S. Dapprich, A.D. Daniels, M.C. Strain, O. Farkas, D.K. Malick, A.D. Rabuck, K. Raghavachari, J.B. Foresman, J.V. Ortiz, Q. Cui, A.G. Baboul, S. Clifford, J. Cioslowski, B.B. Stefanov, G. Liu, A. Liashenko, P. Piskorz, I. Komaromi, R.L. Martin, D.J. Fox, T. Keith, M.A. Al-Laham, C.Y. Peng, A. Nanayakkara, M. Challacombe, P.M.W. Gill, B. Johnson, W. Chen, M.W. Wong, C. Gonzalez, J.A. Pople, Gaussian 03, Revision B.03, Gaussian Inc., Pittsburgh, PA, 2003.

[30] W.R. Wadt, P.J. Hay, J. Chem. Phys. 82 (1985) 284–298.

[31] P.J. Hay, W.R. Wadt, J. Chem. Phys. 82 (1985) 299–310.

[32] P. Pyykkö, N. Runeberg, F. Mendizabal, Chem. Eur. J. 3 (1997) 1451–1457.

[33] E. Cancès, B. Mennucci, J. Tomasi, J. Chem. Phys. 107 (1997) 3032–3041.

[34] A. Bondi, J. Phys. Chem. 68 (1964) 441–451.